HUMBOLDT-UNIVERSITÄT ZU BERLIN

FACULTY FOR MATHEMATICS AND NATURAL SCIENCE I
DEPARTMENT OF PHYSICS

Applied Physics:
Advanced Laboratory

5th experiment:
Z^0-Resonance

date of experiment	14.06.2011
hand in	03.08.2011
advisor	Gerrit Spengler
experimentalists	Lucas Hackl
	Benjamin Maier

Contents

Abstract

We searched for Z^0 bosons produced in electron-positron-collisions of the L3 detector at LEP (CERN) at center-of-mass energies of about $\sqrt{s} \approx 91\,\mathrm{GeV}$. We introduced proper selection criteria to distinguish between $Z^0 \to q\bar{q}$, $Z^0 \to \mu\bar{\mu}$ and underground events, comparing with Monte-Carlo simulations. Using these cuts we were able to determine the mass of the Z^0 boson and – by combining the different values of decay rates – to compute further parameters of the standard model, such as the Z^0 decay width, its life-time, the Weinberg angle and the number of colors in the strong interaction.

1 Introduction

1.1 Theory

1.1.1 Standard Model

The standard model of particle physics is a quantum field theory which includes three of the four fundamental forces, concretely the electromagnetic, the weak and the strong interaction, whereas gravity is not considered. The interactions themselves are described by gauge fields (abelian for the electromagnetic interaction and non-abelian for the other) whose excited states are interpreted as vector bosons. In this picture the subatomic particles we know are described as quantum fields as well. Roughly speaking, the elements in the taylor expansion in the coupling constant of the time evolution operator (using quantum mechanics for fields with its canonical quantization) can be seen as diagrams and the appearing terms as vertices and edges (propagators). This very convenient way of facing the calculation was introduced and developed by R. Feynman in 1949.
A. Salam, S. Glashow and S. Weinberg were able to unify the electromagnetic and the weak interaction within one theory, the theory of the electroweak interaction. From this point of view the gauge bosons of the electroweak interactions are produced by a spontaneous symmetry breaking of the underlying $\mathrm{SU}(2) \times \mathrm{U}(1)_\gamma$ symmetry to $\mathrm{SU}(2) \times \mathrm{U}(1)_{\mathrm{em}}$. Then, the B^0 and W^0 bosons mix up to the real gauge bosons Z^0 and γ, whereas the $W^\pm$ bosons still remain unchanged.
This gauge group predicts one electrically-neutral, massive gauge boson commonly referred as Z^0. The mass m_Z and the percentage of B^0/W^0 mixing (described by the Weinberg angle θ_W) remain as free parameters of the field theory which have to be determined by experimental setups. Furthermore, the relationship of the two couple constants – the electromagnetic one and that of the weak interaction – is determined by the Weinberg angle as well. Exactly these setups were provided by the LEP at CERN (Geneva, Switzerland). We will use the data of about 10 000 scattering events to determine these two parameters of the model. Furthermore, we are able to calculate the decay width of the process which is connected with its lifetime.

1.1.2 Z^0 Resonance

In this experiment we are looking at the process

$$e^+e^- \to Z^0 \to f\bar{f},$$

where f stands for the possible resulting fermions: the leptons e, μ, τ, their neutrinos ν_e, ν_μ, ν_τ and the quarks u, d, c, s, b (note that the center-of-mass energies of the experiment are too small to produce t-pairs). Using Feynman diagrams we can derive the form of the amplitude which contains a factor (because of the massive Z^0 propagator)

$$A \approx \frac{1}{s - M_Z^2 + i M_Z \Lambda_Z}$$

(with the Mandelstam variable $s = p_{e^-}^2 + p_{e^+}^2$). Therefore, it has a pole at $s = M_Z^2$ which we have regulized by introducing the complex term in the numerator. For an s close to M_Z the propability of producing a Z^0 boson increases dramatically. At this energy QED effects are almost eliminated and the processes including Z^0 decay becomes maximal. Because of the propagator the cross section function $\sigma(\sqrt{s})$ has the form of a Breit-Wigner curve

$$\sigma_f = \sigma_0 \frac{s\Gamma_Z^2}{\left(s - M_Z^2\right)^2 + M_Z^2\Gamma_Z^2} \tag{1}$$

1.1.3 Relevant Quantities

The amplitude σ_0 can be calculated considering the decay widths of the initial state (electron e) and the final state (fermion f)

$$\sigma_0 = \frac{12\pi}{M_Z^2\Gamma_Z^2}\,\Gamma_e\Gamma_f, \tag{2}$$

where the fermionic decay width can be evaluated following

$$\Gamma_f = \frac{G_F M_Z^3}{24\pi\sqrt{2}}\left[1 + \left(1 - 4\,|Q_f|\,\sin^2\theta_{\mathrm{W}}\right)^2\right]. \tag{3}$$

Here, $G_F = 1.166 \times 10^{-5}\,\mathrm{GeV}^{-2}$ is Fermi's constant, θ_{W} is the Weinberg mixing angle and Q_f is the fermion's charge (± 1 for leptons $l^\pm$, 0 for their neutrinos, 2/3 for up-kind quarks and -1/3 for down-kind quarks.

1.2 Experimental setup

1.2.1 L3 Detector

As a collaboration of more than 50 international institutes the L3 experiment built the largest known LEP detector. It detects particles from electron-positron-annihilation which happens in the LEP tunnel. The name L3 was chosen due to the fact that it was built up according to the third draft which was handed in. It is optimized for measuring the energy as precisely as possible (for leptons, photons and hadron jets).
The detector consists of a number of smaller detectors.

1.2.2 Luminosity Monitor

This element consists of two electromagnetic calorimeters and two sets of wire chambers which are placed symmetrically on both sides of the interaction point. It provides the opportunity to measure the luminosity by Bhabha scattering with a relative precision of 0.3%. However, the luminosity given for our data was associated with a relative error of 1%.

1.2.3 Track Detector

The track detector enables us to measure the trajectory of a particle. It is made up of cylindric scintillator layers to measure the z-direction (which we put parallel to the incoming beams) and of a drift chamber which ensures a low drift velocity by a low diffusion gas mixture at proper pressure.

1.2.4 Electromagnetic Calorimeter

Since electrons and positrons mainly interact over the electromagnetic force (cascades of annihilation and pair production), this calorimeter must take care of an effective absorbing. In the L3 detector, this is done with semiconductor detectors of the type $Bi_4Ge_3O_{12}$ [5], which effectively analyze these electromagnetic showers.

1.2.5 Scintillation Counters

The scintillation counters consist of 30 plastic counters situated between the electromagnetic and hadronic calorimeters. It is an important element for distinguishing between Z^0 muons and cosmic muons, because the time difference between two events in different scintillators are unequal: While a cosmic muon need about 6 ns (because it passes the whole detector), the Z^0 muon pair, we are interested in, will activate two detectors at the same time.

1.2.6 Hadronic Calorimeter

The hadronic calorimeter has to detect particles which mainly interact over the strong interaction and for this reason can pass the scintillation counter. Their energy can be measured considering total absorption: conclusively, the main materials in the hadronic calorimeters are those with a high mass number A, since these interact strong, as well. In the L3 detector the hadronic chamber is made of several uranium absorber plates. A huge amount of wires ensures that we are able to locate the place of the energy absorption. It acts as a calorimeter and filter at the same time because only non-showering particles will pass.
Since the main particles detected in the hadronic calorimeters are pions, a detection will be associated with the pion mass in the data.

1.2.7 Muonic Calorimeter

The last calorimeter is the muonic calorimeter: Muons are about 200 times heavier and for this reason they are likely to pass the electromagnetic calorimeter (energy absorption is inverse proportional to the mass) and the hadronic one (leptons do not strongly interact). Between hadronic and muonic calorimeter a muon filter is placed which ensures that mainly muons can pass into the last chamber.

1.2.8 Surrounding Magnets

The whole detector is surrounded by a magnetic structure made of iron with a small carbon content. The central field in the magnet is about 0.5 T. By reconstructing the circle trajectory of a particle, one is able to determine its charge (considering the Lorentz force).

2 Data analysis

2.1 Filter criteria

Since the data measured at $\sqrt{s}$ contains all kind of events, it is necessary to find criteria to distinguish between hadronic, muonic and other events. Let P be a set which contains all particles of an event. We modified the event class in our C++ program to calculate certain information for each event set P, concretely:

- Number of particles in the event

$$|P|$$

- Total transversal momentum

$$p_T^t = \sqrt{\sum_{i\in P}\left[(p_i^x)^2 + (p_i^y)^2\right]}$$

- Total momentum

$$p^t = \sqrt{\sum_{i\in P}\left[(p_i^x)^2 + (p_i^y)^2 + (p_i^z)^2\right]}$$

- Total energy

$$E^t = \sum_{i\in P}\sqrt{(p_i^t)^2 + m_i^2}$$

To calculate the efficiency of our cuts we test them with Monte-Carlo simulations done for muonic and hadronic events at $\sqrt{s} = 91.2\,\text{GeV}$ (cf. figures 2-3). For the relative efficiency, which describes the quality of our cuts, we use

$$\varepsilon = \frac{N'}{N},$$

which means that we devide the number of correct selected Monte-Carlo events N' by the total event number N. This is in agreement with [1]. Since this algorithm follows the Bernoulli distribution, the standard deviation of N' is $\sigma = \sqrt{N}/2$. For a confidence interval of 95% we choose the uncertainty to be twice the standard deviation. Hence, the relative efficiency is associated with a statistical error of $\Delta\varepsilon = \frac{1}{\sqrt{N}}$. Its systematic error must be evaluated by varying the selection criteria.
Now, we used cuts which are similar to those of [2].

2.1.1 Selection of hadronic events

Comparizing different tests we finally decided to use the following filter criteria

- Because hadronic events (with a quark-anitquark pair) always consist of jets with a much higher number of particles than the muonic events, we use the number of hits in the hadronic calorimeter as first criterium:

$$|P| > 14$$

- Furthermore we want to select events which have an energy comparable to the center of mass energy. In comparison with the Monte-Carlo simulations we choose the following interval:

$$0.5 < \frac{E^t}{\sqrt{s}} < 1.5$$

- A last criterium which is consistent with the Monte-Carlo simulation is

$$\frac{p_T^t}{p^t} < 0.5$$

We calculate the following relative efficiency:

$$\varepsilon = 0.97 \pm 0.01_{\text{stat}} \pm 0.02_{\text{sys}}$$

The comparison between the Monte-Carlo data and the real data can be seen in figures 6-7.

2.1.2 Selection of myonic events

For the selection of muonic events we decided to use the following filter criteria:

- The event must not be a hadronic event.

- In a first order Feynman diagram, a muonic event only produces a muon pair. However, for higher orders, gluon radiation may cause hadronization and detections in the hadronic calorimeters, as well. But since these processes are suppressed, it is not likely that a jet of many particles will occur. Therefore, the particle number of a muon event should be rather small, yielding the following cut:

$$|P| < 10$$

- Producing a muon pair of total mass $2m$, momentum p and charge q should be conserved. Therefore, we determine a set D out of the event set P as

$$D = \Bigg\{ (i,j) \in P \times P : \\ (m_i = m_j = 0.106\,\text{GeV}) \wedge \\ (q_i = -q_j) \wedge \\ \left(\cos\phi = \frac{\mathbf{p}_i \mathbf{p}_j}{|\mathbf{p}_i|\,|\mathbf{p}_j|} < -0.9 \right) \Bigg\}.$$

  The contributing criterium of P being a muon event is

$$|D| > 0.$$

- Again, we want to select events which have an energy comparable to the center-of-mass energy. By comparison with the Monte-Carlo simulations we choose the following interval:

$$0.8 < \frac{E^t}{\sqrt{s}} < 1.2$$

We calculate the following relative efficiency:

$$\varepsilon = 0.58 \pm 0.01_{\text{stat}} \pm 0.04_{\text{sys}}$$

The comparison between the Monte-Carlo data and the real data can be seen in figures 8-9. It can be stated that the cuts for hadronic events are in higher agreement than these for muonic events. Nevertheless, they can be taken to compute the muonic cross sections.

C.M. Energy $\sqrt{s}\,/\,\mathrm{GeV}$	Luminosity $L\,/\,\mathrm{nb}^{-1}$	Hadronic Event Counts N^{Had}	Hadronic Cross Sections $\sigma^{\mathrm{Had}}\,/\,\mathrm{nb}$	Muonic Event Counts N^{μ}	Muonic Cross Sections $\sigma^{\mu}\,/\,\mathrm{nb}$
89.48 ± 0.89	179.3 ± 1.8	1745	10.04 ± 0.25	72	0.691 ± 0.050
91.33 ± 0.91	135.9 ± 1.4	3896	29.57 ± 0.74	140	1.773 ± 0.127
93.02 ± 0.93	151.1 ± 1.5	2085	14.23 ± 0.36	85	0.968 ± 0.069

Table 1: Extracted event counts and calculated cross sections

2.2 Calculation of Breit-Wigner Parameters

The curve of the cross section $\sigma(\sqrt{s})$ has the form of a Breit-Wigner distribution where the resonance takes place at M_Z. Precisely speaking we have to introduce a further correction caused by effects of quantum electrodynamics, which is done by a program written for [1].
To calculate the cross section we use

$$\sigma = \frac{N}{L},$$

with L being the integrated luminosity. As mentioned, it is associated to a relative uncertainty of 1 % (as explained in [1]). The measurement of the luminosity is done by Bhabha scattering at small scattering angles with specific detector components. This is a pure QED process and for this reason independent from the Z^0 properties we will compute. We use the values given in [1], combined in table 1.
To determine the number of events N we analyze the data with the cuts above, gaining N'. We do not find a significant background. For this reason we try to estimate the background in a similar way as explained in [2] on p. 38 (hadronic events) and 41 (muonic events): We subtract the number of background events ($p = 0.15\,\%$ of N' for hadronic events and $p = 0.7\,\%$ of N' for muonic events) and divide by our relative efficiency, yielding

$$N = \frac{(1-p)N'}{\varepsilon},$$

respectively

$$\sigma = \frac{(1-p)N'}{\varepsilon L}.$$

The Gaussian error propagation was used to evaluate the cross section's uncertainty. Using these formulas, we gain the results shown in table 1.
Now we are able to perform two fits to gain the events' cross section curves. Since the algorithm of minimizing χ^2 is performed with zero degrees of freedom, it is rather a calculation with error propagation of the Breit-Wigner parameters than a proper fit. The results of this calculation may be seen in table 2 and figure 1.

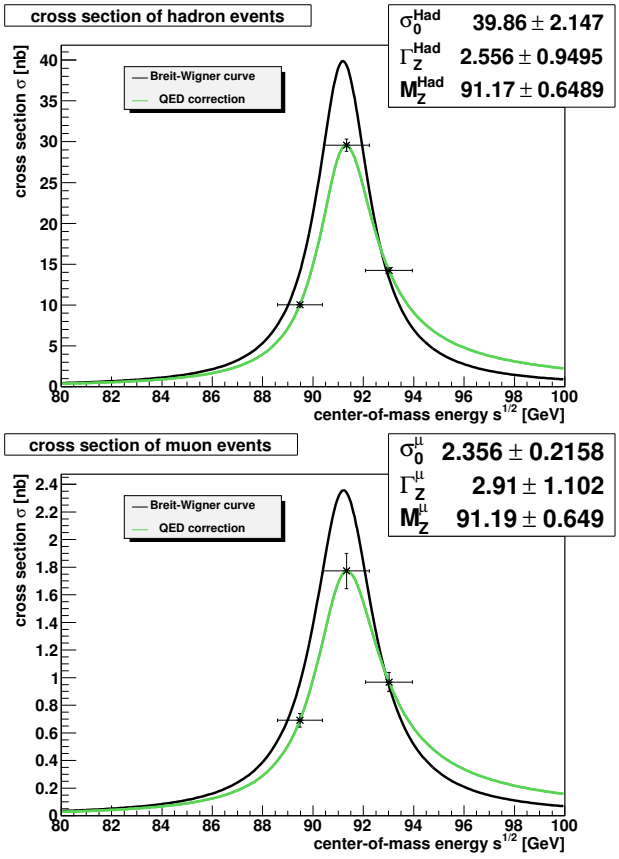

Figure 1: Breit-Wigner curves determined from the calculated cross sections. The results are shown in table 2.

Parameter	Hadronic Result (Had)	Muonic Result (μ)
$\sigma_0\,/\,\mathrm{nb}$	39.9 ± 2.4	2.46 ± 0.42
$\Gamma_Z\,/\,\mathrm{GeV}$	2.56 ± 0.95	3.13 ± 1.31
$M_Z\,/\,\mathrm{GeV}$	91.2 ± 0.7	91.1 ± 0.7

Table 2: Parameters gained from Breit-Wigner calculation

2.3 Derived parameters

In this part we will calculate the free parameters of the standard model which are determined by the Breit-Wigner parameters. When not stated in another way, we used the Gaussian method of error propagation by accounting all parameters.

2.3.1 Properties of the Z^0 Boson

Since both the results (gained from muonic and hadronic cross sections) are of equal value, we are able to calculate weighted means[1], yielding

$$\begin{aligned} M_Z &= (91.2 \pm 0.5)\,\mathrm{GeV} \\ \Gamma_Z &= (2.7 \pm 0.7)\,\mathrm{GeV} \\ \tau_Z &= (2.4 \pm 0.6) \times 10^{-25}\,\mathrm{s} \end{aligned}$$

The Z^0 life-time was calculated using the formula $\tau = \hbar/\Gamma$.

2.3.2 Leptonic Decay Width

From Muonic Cross Sections Since both, the initial and the final state of the reaction, are leptonic states with $|Q_f| = 1$, we are able to evaluate the leptonic decay width using equation (2) to

$$\Gamma_e^\mu = M_Z^\mu \Gamma_Z^\mu \sqrt{\frac{\sigma_0^\mu}{12\pi}},$$

yielding the result

$$\Gamma_e^\mu = (106 \pm 41)\,\mathrm{MeV}.$$

The superscript μ denotes that the quantity was gained using the results from the muonic cross sections.

From Hadronic Cross Sections Again, using equation (2), we are able to compute the amplitude σ_0 of the hadronic cross section

$$\sigma_0^{\mathrm{Had}} = \frac{12\pi\Gamma_e\Gamma_{\mathrm{H}}}{\left(M_Z^{\mathrm{Had}}\Gamma_Z^{\mathrm{Had}}\right)^2}.$$

The superscript Had denotes that the quantity was gained using the results from the hadronic cross sections. Since Γ_{H}, the hadronic decay width is not known, we can use the fact that the Z^0 decay width is the sum of all decay widths

$$\Gamma_Z^{\mathrm{Had}} = \Gamma_{\mathrm{H}} + 3\Gamma_\nu^{\mathrm{Had}} + 3\Gamma_e^{\mathrm{Had}}.$$

Due to the neutral charge of neutrinos, we are able to calculate the neutrino decay width using equation (3)

$$\Gamma_\nu^{\mathrm{Had}} = \frac{G_F\left(M_Z^{\mathrm{Had}}\right)^3}{12\pi\sqrt{2}}.$$

Combining all the equations above, we arrive at the leptonic decay width

$$\begin{aligned} \Gamma_e^{\mathrm{Had}} = &-\frac{1}{2}\left(\frac{G_F\left(M_Z^{\mathrm{Had}}\right)^3}{12\pi\sqrt{2}} - \frac{\Gamma_Z^{\mathrm{Had}}}{3}\right) \\ &\pm\sqrt{\frac{1}{4}\left(\frac{G_F\left(M_Z^{\mathrm{Had}}\right)^3}{12\pi\sqrt{2}} - \frac{\Gamma_Z^{\mathrm{Had}}}{3}\right)^2 - \frac{\sigma_0^{\mathrm{Had}}\left(M_Z^{\mathrm{Had}}\right)^2\left(\Gamma_Z^{\mathrm{Had}}\right)^2}{36\pi}} \end{aligned}$$

We are gaining two results using this equation. Hence, we have to compare them with the value from literature $\Gamma_e = (83.6 \pm 0.8)\,\mathrm{MeV}$ to determine the physically most likely result

$$\Gamma_e^{\mathrm{Had}} = (81 \pm 21)\,\mathrm{MeV}.$$

Final Result Again, both, the muonic and the hadronic results, are of equal value. Hence, we have no reason to neglect one of them and calculate the weighted mean:

$$\Gamma_e = (87 \pm 19)\,\mathrm{MeV}.$$

2.3.3 Weinberg Angle

The electroweak mixing angle, respectively its squared sine $S_\theta^2 = \sin^2\theta_{\mathrm{W}}$, can be determined using two different equations. The first two results may be evaluated using equation (3)

$$S_{\theta,\pm}^2 = \frac{1}{4}\left(1 \pm \sqrt{\frac{\Gamma_e\, 24\pi\sqrt{2}}{G_F M_Z^3} - 1}\right). \tag{4}$$

Referring to [6], the third result can be calculated using the equation

$$S_{\theta,3}^2 = 1 - \frac{M_W^2}{M_Z^2},$$

where $M_W = (80.399 \pm 0.023)\,\mathrm{GeV}$ is the $W^\pm$ boson mass, taken from [7]. For calculating the uncertainty of the first formula we used a maximum error estimation[2], since the used quantities are related to each other. The uncertainty of the second formula is calculated with the Gaussian method, as usual. Finally, using the weighted means of the needed parameters, we gain the results

$$\begin{aligned} S_{\theta,+}^2 &= 0.303 \pm 0.143, \\ S_{\theta,-}^2 &= 0.197 \pm 0.143, \\ S_{\theta,3}^2 &= 0.223 \pm 0.008. \end{aligned}$$

[1] We are using the formulas $\bar{x} = \sum_i w_i x_i / \sum_i w_i$ and $\Delta x = 1/\sqrt{\sum_i w_i}$ with weights $w_i = 1/\Delta x_i^2$

[2] i.e. the formula $\Delta f(\mathbf{x}) = \sum_{i\in\mathbf{x}} \Delta x_i \left|\frac{\partial f}{\partial x_i}\right|$

Quantity	Equations (3) and (5)	Equation (3) with Weinberg +	−	3
Γ_ν / GeV	0.1658 ± 0.0025			
Γ_H / GeV	1.97 ± 0.78			
Γ_d / GeV		0.11 ± 0.02	0.128 ± 0.025	0.124 ± 0.003
Γ_u / GeV		0.086 ± 0.013	0.101 ± 0.032	0.097 ± 0.003

Table 3: Calculated decay widths

Compared to the value given in the literature $S^2_\theta = 0.23120 \pm 0.00015$ [8], the results $S^2_{\theta,-}$, $S^2_{\theta,3}$ seem to be more likely. However, all the values are right within in their uncertainty range. Thus, we have to compute all following results with all the values.

2.3.4 Number of Quark Colors

This quantity N_C is a factor in the decay width of quarks Γ_H, i.e.

$$\Gamma_H = N_C K_{QCD} (2\Gamma_u + 3\Gamma_d),$$

where $K_{QCD} \approx 1.04$ is a factor from Feynman diagrams of higher orders for gluon radiation [1]. Again, the decay width of hadron events can be examined from the total decay width using

$$\Gamma_H = \Gamma_Z - 3\Gamma_\nu - 3\Gamma_e, \tag{5}$$

summing up

$$N_C = \frac{\Gamma_Z - 3\Gamma_\nu - 3\Gamma_e}{K_{QCD} (2\Gamma_u + 3\Gamma_d)}.$$

The quantities Γ_u, Γ_d and Γ_ν can be computed with the electroweak mixing angle using equation (3). Since many of the quantities are related we are using a maximum error estimation again, yielding the decay width results shown in table 3. Finally we gain the values

$$N_{C,+} = 3.7 \pm 2.1,$$
$$N_{C,-} = 3.2 \pm 2.0,$$
$$N_{C,3} = 3.4 \pm 1.4.$$

Although all values are in agreement with the expected value $N_C = 3$, they are too high and their uncertainties are rather large, too.

3 Conclusion

We were successfully able to extract the number of events using the cuts described in section 2.1, to gain the cross sections, the Breit-Wigner parameters, the leptonic decay width, the electroweak mixing angle and the number of quark colors, summing up the physically most likely results in table 4. They are in agreement with the literature.

quantity		measured	literature
Z^0 mass:	M_Z / GeV	91.2 ± 0.5	91.1876 ± 0.0021
Z^0 decay width:	Γ_Z / GeV	2.7 ± 0.7	2.4952 ± 0.0023
Z^0 life time:	$\tau_Z / 10^{-25}$ s	2.4 ± 0.6	2.6378 ± 0.0024
total hadronic decay width:	Γ_H / GeV	2.0 ± 0.8	1.7444 ± 0.0020
leptonic decay width:	$\Gamma_{e=\mu=\tau}$ / GeV	0.09 ± 0.02	0.0833 ± 0.0010
neutrino decay width:	Γ_ν / GeV	87 ± 19	0.1663 ± 0.0005
electroweak mixing angle:	$S^2_{\theta,-}$	0.197 ± 0.143	0.23120 ± 0.00015
	$S^2_{\theta,3}$	0.223 ± 0.008	0.23120 ± 0.00015
number of quark colors:	$N_{C,-}$	3.2 ± 2.0	3
	$N_{C,3}$	3.4 ± 1.4	3

Table 4: Final results and reference values from literature [7] and [8]

However, the results are partly associated with very large uncertainties. At first, these come through the high systematical errors of the relative efficiency, which is hard to estimate, since a variation of filter criteria may lead to a significantly other result. Furthermore, large errors are probably produced during the Breit-Wigner "fit". Since the procedure is not a real fit (zero degrees of freedom), the results including their errors may not be computed in the right way. It would be helpful to have more data points to perform a real fit.
In addition to this, the correlation matrix of the parameters may not be right, too. With a proper fit, it would be possible to perform a correlated error propagation which could lead to smaller errors. Furthermore, it would be possible to perform a correlated error analysis for all the quantities.
Another systematical error may be produced due to the cut for muon pair production. Looking at the Monte-Carlo simulation for muonic events, there are a number of events which do not fulfill this condition (no muons are detected). Here, it would be useful to know in detail, how the Monte-Carlo simulation is done. Maybe events of higher order, which produce muon pairs in loops, are meant to be muonic events, as well, although the final products do not contain muons. Considering this aspect, the muon cuts' efficiency may be raised to gain better results.

Literature

[1] M. zur Nedden, *Anleitung zum Versuch Z^0-Resonanz im Fortgeschrittenen-Praktikum*, 2010

[2] O. Adrinai et al., *Results from the L3 Experiment at LEP*, Physics Reports 236(1993)1, 1993

[3] H. Schopper, *Die Ernte nach einem Jahr LEP-Betrieb*, Physikalische Blätter 47(1991)907, 1991

[4] http://hepsrv.phy.ncu.edu.tw:8000/detector_all/picture/l3detector_1.JPG (Luminosity picture)

[5] Y. Karyotakis, *The L3 Electromagnetic Calorimeter*, LAPP-EXP-95.02, February 1, 1995 (http://citeseerx.ist.psu.edu/viewdoc/download?doi=10.1.1.143.2428&rep=rep1&type=pdf)

[6] H. Lacker, *Vorlesung: Einführung in die Kern- und Elementarteilchenphysik*, Humboldt-Universität zu Berlin, 2011 http://www-eep.physik.hu-berlin.de/teaching/lectures/ss2011/EINF_KET_SS11/vl26

[7] Particle Data Group, *Particle Physics Booklet*, July 2010, p. 8

[8] Wikipedia Foundation, *Weinberg angle* http://en.wikipedia.org/wiki/Weinberg_angle, 31.07.2011

Appendix

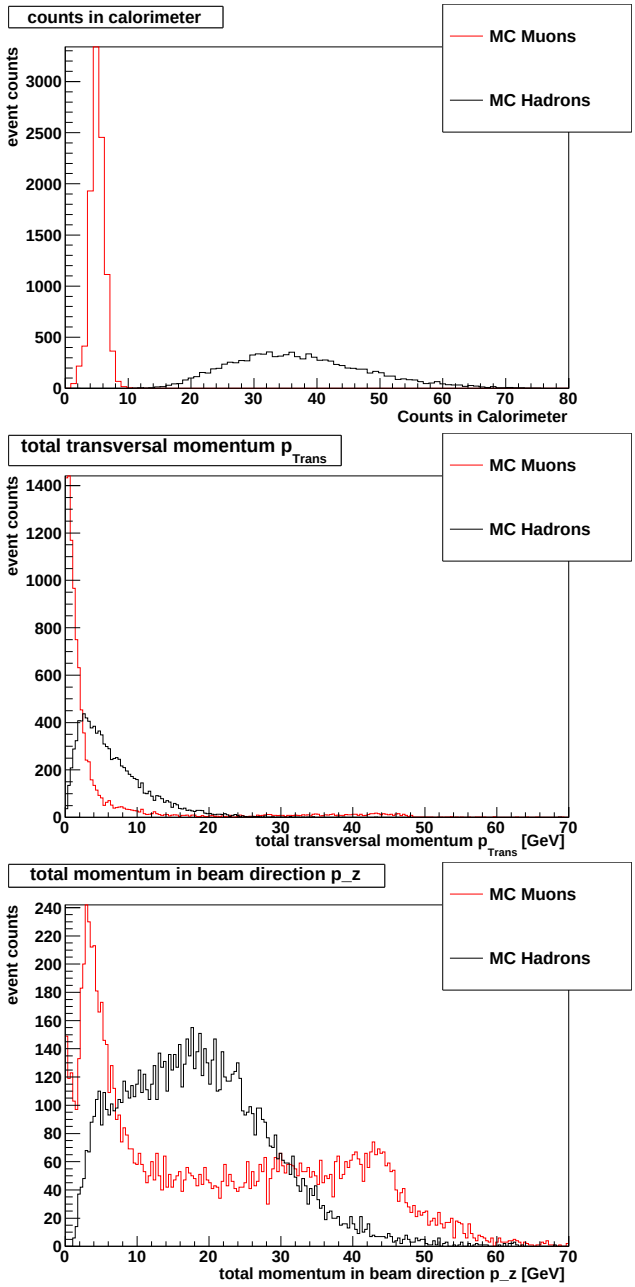

Figure 2: Various event properties gained by Monte-Carlo simulations

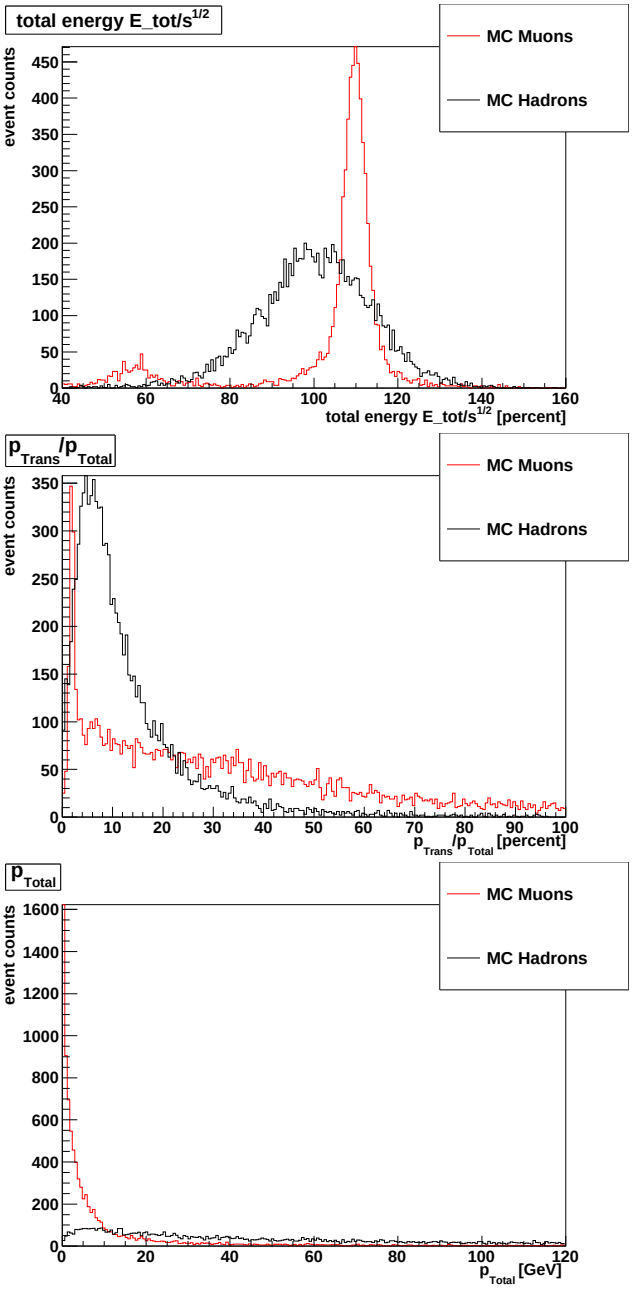

Figure 3: Various event properties gained by Monte-Carlo simulations

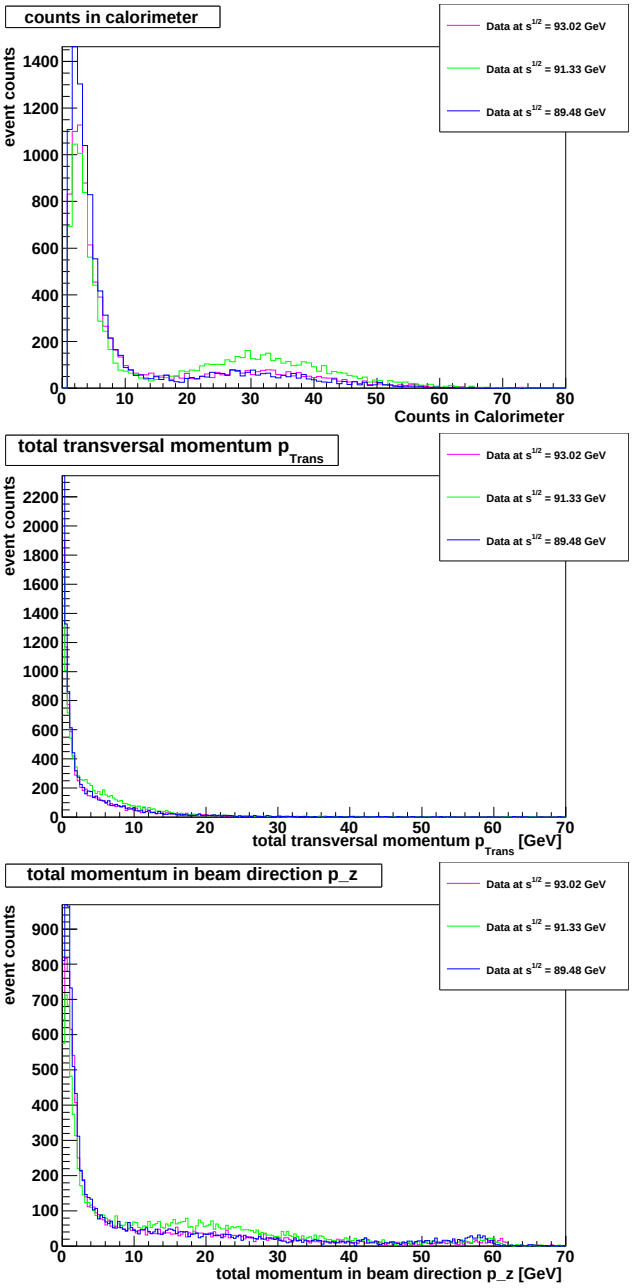

Figure 4: Various event properties of the real data

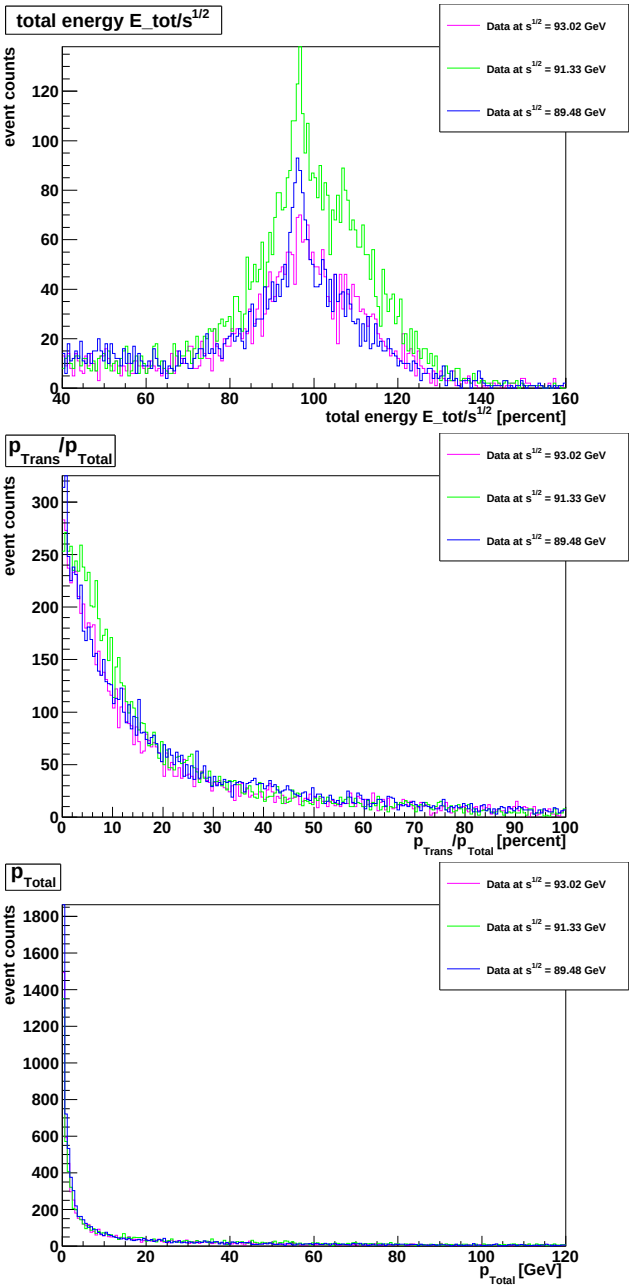

Figure 5: Various event properties of the real data

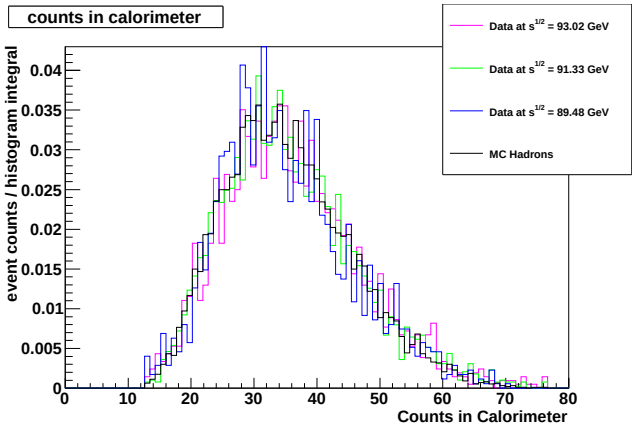

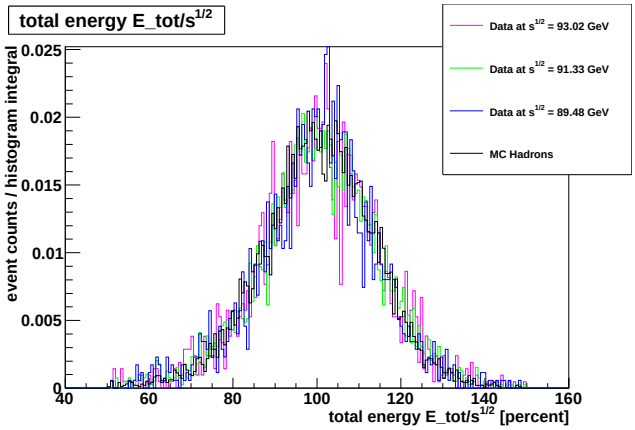

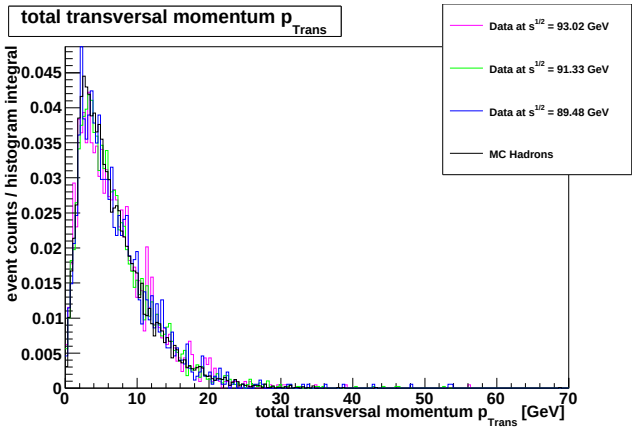

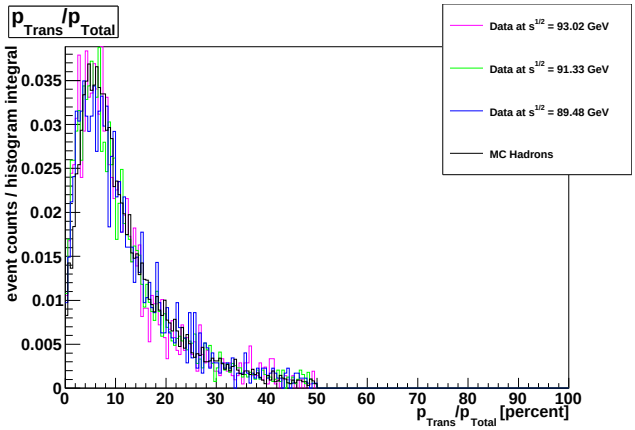

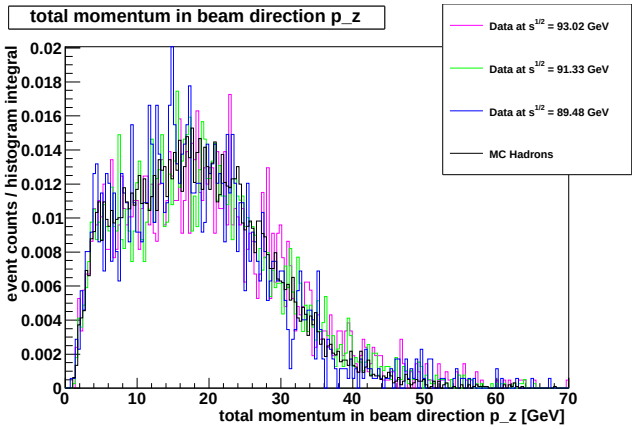

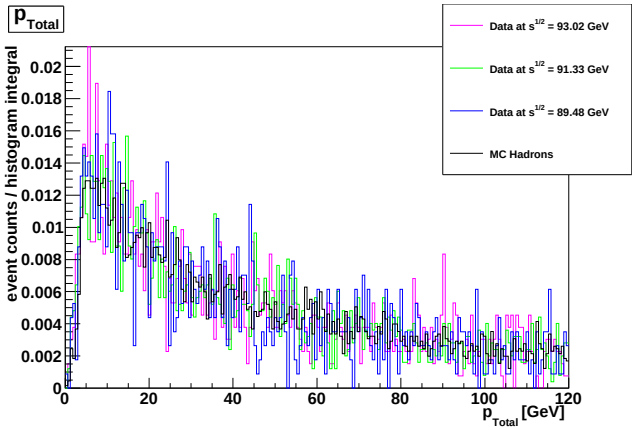

Figure 6: Various event properties of the data gained with cuts for hadrons

Figure 7: Various event properties of the data gained with cuts for hadrons

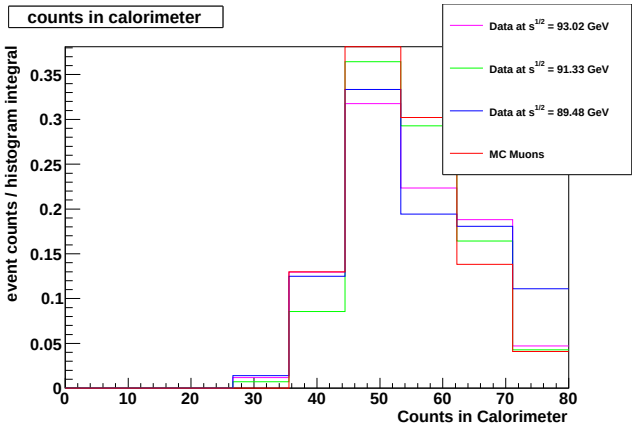

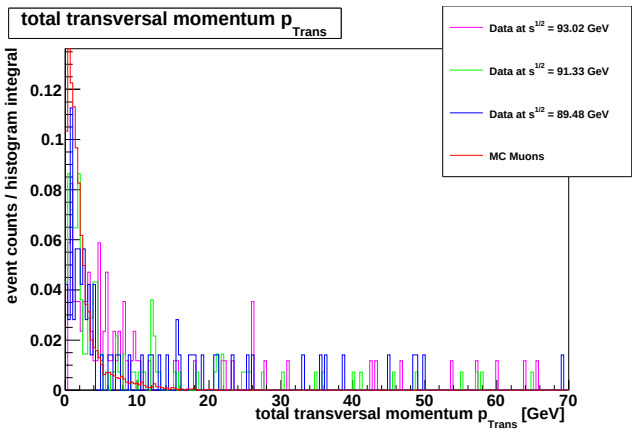

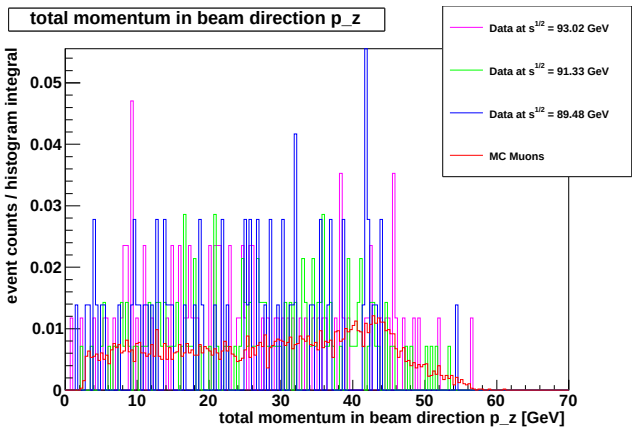

Figure 8: Various event properties of the data gained with cuts for hadrons

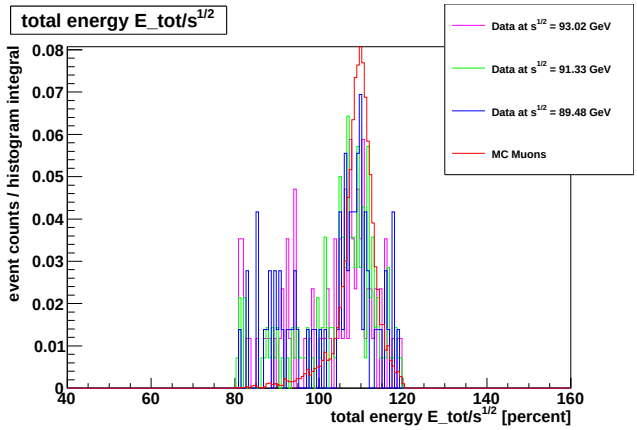

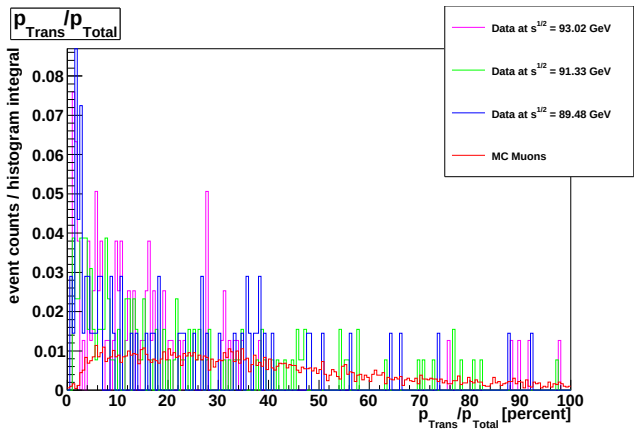

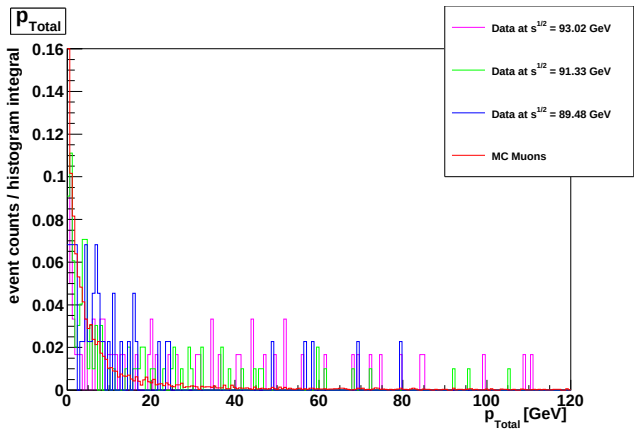

Figure 9: Various event properties of the data gained with cuts for hadrons